Title

Revealing the Phase Separation Behavior of Thermodynamically Immiscible Elements in a Nanoparticle

Journal

Nano Letters, 21(15)

ISSN

1530-6984

Authors

Chen, Peng-Cheng

Gao, Mengyu

Yu, Sunmoon

et al.

Publication Date

2021-08-11

DOI

10.1021/acs.nanolett.1c02225

Peer reviewed

Revealing the Phase Separation Behavior of Thermodynamically Immiscible Elements in a Nanoparticle

Peng-Cheng Chen,[†,§,‡] Mengyu Gao,[‖,×,‡] Sunmoon Yu,[‖,#] Jianbo Jin,[§] Chengyu Song,[⊥] Miquel Salmeron,[‖,×] Mary C. Scott,[‖,⊥] and Peidong Yang[*,†,§,‖,×,#]

† Kavli Energy Nanoscience Institute, University of California, Berkeley, California 94720, United States

§ Department of Chemistry, University of California, Berkeley, California 94720, United States

‖ Department of Materials Science and Engineering, University of California, Berkeley, California 94720, United States

× Materials Sciences Division, Lawrence Berkeley National Laboratory, Berkeley, California 94720, United States

Chemical Sciences Division, Lawrence Berkeley National Laboratory, Berkeley, California 94720, United States

⊥ National Center for Electron Microscopy, Molecular Foundry, Lawrence Berkeley National Laboratory, Berkeley, California 94720, United States

*Corresponding Author: Peidong Yang, *email address*: p_yang@berkeley.edu

KEYWORDS

Heterostructured nanoparticle, phase separation, thermodynamics, electron tomography

ABSTRACT

Phase-separation is commonly observed in multimetallic nanomaterials, yet it is not well understood how immiscible elements distribute in a thermodynamically stable nanoparticle. Herein, we studied the phase-separation of Au and Rh in nanoparticles using electron microscopy and tomography techniques. The nanoparticles were thermally annealed to form thermodynamically stable structures. HAADF-STEM and EDS characterizations reveal that Au and Rh segregate into two domains while their miscibility is increased. Using aberration-corrected HAADF-STEM and atomic electron tomography, we show that the increased solubility of Au in Rh is achieved by forming Au clusters and single atoms inside the Rh domains and on the Rh surface. Furthermore, based on the three-dimensional reconstruction of a AuRh nanoparticle, we can directly visualize the uneven interface that is embedded in the nanoparticle. The results advance our understanding on the nanoscale thermodynamic behavior of metal mixtures, which is crucial for the optimization of multimetallic nanostructures for many applications.

MAIN TEXT

Phase-separation is a typical thermodynamic phenomenon that can be found in multimetallic materials.[1,2] Metals with a highly positive enthalpy of mixing are energetically unfavorable to be mixed with each other, which usually segregate into different domains.[2-4] Such phenomenon is particularly ubiquitous in nanoparticles composed of immiscible elements. In addition, the small size and high surface-area-to-volume ratio of nanoparticles impart them high flexibility in structural transformation.[5-7] Despite various kinetic structures that nanoparticles may have based on the delicate design of synthetic methods, the application of nanoparticles such as catalysis often triggers their structural evolution to reach a thermodynamically stable state once sufficient external energy (e.g., thermal energy, electrochemical bias) is provided to the systems.[8-14] Consequently, phase separation is broadly observed in nanoparticles comprising immiscible elements.[6,12,15-20]

Compared with phase separation at the bulk scale, one notable difference at the nanoscale is the enhanced miscibility between incompatible metals.[21] For instance, the miscibility gaps between incompatible metals such as Pt-Rh, Au-Ir, and Ag-Ni are found to shrink when the particle size decreases.[22-25] The miscibility change is generally ascribed to the increased surface effect on nanoparticles. Specifically, atoms on the particle surface have fewer neighboring atoms than those in bulk, which results in a decrease of the interaction energy between the immiscible elements and hence facilitates their mixing.[23,26-30] The atomic ensemble in multimetallic nanoparticles may also compress and create strains in order to reduce the high surface energy,[31,32] which further complicate the thermodynamic behavior of metals and affect their separation at the nanoscale. While phase-separation has been reported in many types of metal nanoparticles, it remains poorly understood how the immiscible metals distribute in a thermodynamically stable nanoparticle and how the increased miscibility affects the elemental distribution. Understanding the nanoscale thermodynamic behavior will be crucial for designing phase-separated nanoparticles that can be used for a variety of fields including catalysis,[15,33,34] plasmonics,[35,36] magnetics,[37,38] and biological imaging.[39]

Herein, using Au-Rh nanoparticles as a model system, we investigated the phase separation behavior of two thermodynamically immiscible elements in nanoparticles of size ranging from 4 to 12 nm, a size regime that is commonly used for nanoparticle catalysts. High-angle annular dark-field scanning transmission electron microscopy (HAADF-STEM) and energy dispersive x-ray

spectroscopy (EDS) were combined to show that, thermodynamically, Au and Rh segregate into two domains in a nanoparticle while their miscibility in the nanoscale regime is increased. Electron tomography was utilized to reveal the distribution of Au and Rh in a nanoparticle in a three-dimensional (3D) manner. The results not only reveal the distribution of Au and Rh in the particles, but also unravel the topographic morphology of an interface that is embedded in a heterostructured nanoparticle.

According to bulk phase diagram, Au and Rh are immiscible elements, which will form two phases that are virtually monometallic at temperatures lower than 800 °C (each element phase contains < 1% of the other element).[40] In this work, thermal treatment was used to obtain thermodynamic AuRh systems. To assess the efficacy of the thermal treatment, we first prepared a Au-Rh bulk film sample by drop-casting a mixture of gold(III) chloride and rhodium(III) nitrate onto a quartz substrate and thermally annealing the quartz substrate under flowing Ar/H_2 at temperatures as high as 500 °C (see supporting information). X-ray diffraction (XRD) pattern of the annealed sample shows two sets of peaks that can be attributed to face-centered cubic (fcc) Au and fcc Rh crystal structures, respectively (Fig. S1), confirming the efficacy of the annealing process in triggering the thermodynamic phase-separation between Au and Rh. Next, we synthesized AuRh nanoparticles via nanoreactor-mediated synthesis and applied the same thermal treatment to the nanoparticles. Specifically, polymer micelles were utilized as nanoreactors to mediate the nanoparticle synthesis (Fig. 1).[41] The micelles were made by dissolving polystyrene-*b*-poly(2-vinyl pyridine) (PS-*b*-P2VP) in toluene. Metal precursors were sequentially loaded into the micelles by coordinating them with the pyridyl group of the polymers. Following precursor loading, the micelles were spin-coated onto a substrate and successively treated with plasma etching and thermal annealing to decompose the micelle templates and create single AuRh nanoparticles within each micelle (Fig. 1B and S2-S5). The size and composition of nanoparticles were controlled by adjusting the amount and ratio of metal precursors in each micelle reactor, which determines the available metal ions for forming nanoparticles.

To investigate the thermodynamic state of Au and Rh at the nanoscale, HAADF-STEM, EDS, and high-resolution transmission electron microscopy (HRTEM) characterizations were performed on the synthesized nanoparticles. As shown in Figure 1D, HAADF-STEM characterization suggests the formation of heterostructured AuRh nanoparticles (4-12 nm). The

brightness contrast between the two domains that constitutes the heterodimers is due to the atomic number contrast between Au and Rh. HRTEM characterization of a AuRh nanoparticle validates the segregation between Au and Rh (Fig. 1C). Fast Fourier transformation (FFT) of the Au domain indicates that it is oriented along the [011] zone axis of a fcc Au crystal structure, and FFT of the Rh domain shows reflections corresponding to Rh (111) planes. While two distinct lattice structures, corresponding to fcc Au and fcc Rh, respectively, were found in individual AuRh nanoparticles, no specific lattice orientation was observed between the Au and Rh domains (Fig. S6). The phase separation between Au and Rh in the nanoparticles was further evidenced by EDS elemental mapping. As shown in Figure 1D, 2, and S7, AuRh nanoparticles possess a dimeric heterostructure with one domain mainly composed of Au and the other composed of Rh. In order to understand how thoroughly Au and Rh are separated in the particles, we calculated the Pearson's colocalization coefficient (PCC) of the element maps of Au and Rh (Fig. 2A). The PCC values have a range between -1 and 1, where 1 is for two perfectly and linearly related images, 0 is for uncorrelated images, and -1 is for inversely related images.[42] Remarkably, the PCC values of Au and Rh are found between 0.06-0.12, suggesting partial mixing of Au and Rh in the nanoparticle. Moreover, EDS spectra of the Au and Rh domains in a single nanoparticle (Fig. 2B and 2C) as well as the EDS line-scan across the two domains (Fig. 2D) also corroborate the presence of one element in the other element's domain. To quantify the increased miscibility, we further calculated the composition of the Au and Rh domains based on the EDS measurement of 25 AuRh nanoparticles (Fig. S8). Compared with the bulk scenario, the Au content in the Rh domains is increased to ~15% while the Rh content in the Au domains is increased to ~7% (Fig. 2E). Taken together, these studies confirm that Au and Rh phase separate in a thermodynamically stable nanoparticle while their miscibility is clearly increased.

In an attempt to unveil how Au and Rh atoms are organized in a nanoparticle to adopt the increased miscibility, we used aberration-corrected STEM to characterize the AuRh nanoparticles. As shown in Figure 3A and S9, the large atomic number difference between Au and Rh atoms leads to their brightness contrast in the STEM images, making them differentiable at the atomic scale. In consistence with the EDS results, Au clusters and single atoms are found in the Rh domains of the AuRh heterodimers (Fig. 3A and S9). Since HAADF-STEM is a two-dimensional (2D) projection method, it is challenging to identify whether the observed Au species are located inside the Rh domain or on the Rh surface. In this regard, we leveraged atomic electron

tomography,[43] a three-dimensional reconstruction method based on the aberration-corrected STEM, to reveal the distribution of Au and Rh in a nanoparticle from a three-dimensional perspective. A series of STEM images were acquired from a single nanoparticle with varied tilting angles from approximately -60° to 60° (Fig. S10 and S11). Based on these images, a 3D model was reconstructed using the GENFIRE algorithm (see supporting information).[44] As shown in Figure 3B, Video S1, and Video S2, Au clusters can be found both in the Rh domain and on the surface of the Rh domain. The enrichment of Au atoms on Rh surface is presumably owing to the minimization of surface energy since Au possesses a lower surface energy than Rh.[12,45,46] Based on the 3D reconstructed result, we can also break down the nanoparticle into a set of slices along the direction perpendicular to the 2D imaging plane (Fig. 3C and Video S3). From the bottom slice to the top slice (Fig. 3C panel 1-4 and 3D), one can clearly see that in addition to Au single atoms, Au clusters of size between 1-3 nm are present on the edge of the Rh domain as well as inside the Rh domain. Through the combination of HAADF-STEM 2D imaging and 3D reconstruction (Fig. 3 and S9), we conclude that the Au solute is located both in the Rh domain and on the Rh surface in the form of clusters and single atoms. For the distribution of Rh solute in the Au domains, experimentally it is hard to resolve it based on the HAADF-STEM characterization due to the high brightness of Au atoms in the STEM images, which generates a bright background when we try to distinguish the Rh atoms in the Au domains (Fig. S12). Given the higher cohesive energy and surface energy of Rh atoms than Au, we deduce that the increased solubility of Rh in Au is possibly realized by forming Rh clusters and single atoms mainly inside the Au domains.

One important structural feature of heterostructured nanoparticles is the solid-state interface, which has attracted extensive interest due to its significance in modulating the catalytic and plasmonic properties of nanoparticles.[15,17,18,33-36] When the interfaces are incoherent or irregular, it is challenging to characterize them with electron microscopy because many of the interfaces do not have a well-defined lattice structure that can be resolved using 2D imaging methods. In the case of AuRh nanoparticles, we observed some of the nanoparticles possessing non-flat interfaces that are embedded in the particles. HAADF-STEM images of these particles show blurry interfacial regions (Fig. 4A and S9B), in contrast with the distinct transition between Au and Rh domains in nanoparticles with flat interfaces (Fig. S9A). To resolve the topographic morphology of the embedded uneven interface, we applied an algorithm on the reconstructed particle to make the interface visualizable (see supporting information). Specifically, since the

contrast between Au-rich domain and Rh-rich domain are distinctive in the reconstructed structure (Video S1-S3), the interface can be identified by calculating the gradient of the contrast, where high numerical value is taken to be a signature of the Au-Rh interface. Based on the calculated results, Z-slices of the particle were generated with the contour line of the Au domain highlighted in each slice (Fig. 4 and Video S4). As shown in Figure 4B and 4C, the topographic morphology of the phase boundary is highly irregular. At a relatively low Z position, the contour line of the interface protrudes from the Au domain to the Rh domain (Fig. 4B, panel 1). Moving up along the Z direction, the Z-slices show that the protruding part of the interface gradually retracts, resulting in a flat interface inside the particle (Fig. 4B, panels 2-5). Further moving up to a relatively high Z position, the Z-slices show the retraction of another part of the interface, which leads to a protrusion from the Rh domain to the Au domain (Fig. 4B, panels 6-9). As such, the irregular interface is resolved and visualized from a 3D perspective. Taken together, the tomographic study on the AuRh system has provided a comprehensive insight into their thermodynamic distribution in a nanoparticle.

In summary, we have investigated the phase separation behavior of immiscible elements in thermodynamically stable nanoparticles using Au and Rh as a model system. Analytical electron microscopy and atomic electron tomography were combined to reveal the increased miscibility between Au and Rh at the nanoscale, the distribution of Au and Rh in heterostructured nanoparticles, and the topographic morphology of phase boundaries that are embedded in the nanoparticles. Understanding the structure of phase-separated nanoparticles is fundamentally important because the function of the nanoparticles is often dictated by their surface and interfacial structures. Given the importance of phase-separated nanoparticles in a variety of fields,[15,33-39] this work not only advances our understanding on the nanoscale thermodynamic behavior of metal mixtures, but also provides important guidelines for the design of phase-separated nanostructures that can be useful for catalysis, plasmonics, magnetics, and many other applications.

ASSOCIATED CONTENT

Supporting Information.

The Supporting Information is available free of charge on the ACS Publications website.
Experimental section, XRD pattern of AuRh bulk samples, TEM images tracing the micelle-mediated synthesis process, XPS analysis of nanoparticles, HRTEM images of nanoparticles, HAADF-STEM images of nanoparticles, and EDS analysis of nanoparticles.
Video S1: Tomography reconstruction of a AuRh nanoparticle
Video S2: Tomography reconstruction of a AuRh nanoparticle with the intensity histogram of the associated color map modified to highlight the Au-rich domain
Video S3: Z-slices of a 3D-reconstructed AuRh nanoparticle
Video S4: Z-slices of a AuRh nanoparticle with the contour lines of the Au domain highlighted

AUTHOR INFORMATION

Corresponding Author

*Peidong Yang; Email: p_yang@berkeley.edu

Author Contributions

The manuscript was written through contributions of all authors. All authors have given approval to the final version of the manuscript. ‡These authors contributed equally.

Notes

The authors declare no competing financial interest.

ACKNOWLEDGMENT

This work was partially supported by the U.S. Department of Energy, Office of Science, Basic Energy Sciences, Materials Sciences and Engineering Division under Contract No. DE-AC02-05-CH11231 within the Structure and Dynamics of Materials Interfaces program KC31SM. P.-C.C. acknowledges support from Kavli ENSI Heising-Simons Fellowship. S.Y. acknowledges support from Samsung Scholarship. J.J. acknowledges fellowship support from Suzhou Industrial Park. The authors thank Dr. P. Ercius for helpful discussion on tomography. Work at the Molecular

Foundry was supported by the Office of Science, Office of Basic Energy Sciences, of the U.S. Department of Energy under Contract No. DE-AC02-05CH11231.

REFERENCES

(1) Calvo, F., Thermodynamics of nanoalloys. *Phys. Chem. Chem. Phys.* **2015,** *17* (42), 27922-27939.

(2) Zhang, R. F.; Kong, X. F.; Wang, H. T.; Zhang, S. H.; Legut, D.; Sheng, S. H.; Srinivasan, S.; Rajan, K.; Germann, T. C., An informatics guided classification of miscible and immiscible binary alloy systems. *Sci. Rep.* **2017,** *7*, 9577.

(3) Zhang, R. F.; Zhang, S. H.; He, Z. J.; Jing, J.; Sheng, S. H., Miedema Calculator: A thermodynamic platform for predicting formation enthalpies of alloys within framework of Miedema's Theory. *Comput. Phys. Commun.* **2016,** *209*, 58-69.

(4) Ferrando, R.; Jellinek, J.; Johnston, R. L., Nanoalloys: From theory to applications of alloy clusters and nanoparticles. *Chem. Rev.* **2008,** *108* (3), 845-910.

(5) Hodges, J. M.; Morse, J. R.; Williams, M. E.; Schaak, R. E., Microscopic Investigation of Chemoselectivity in Ag-Pt-Fe3O4 Heterotrimer Formation: Mechanistic Insights and Implications for Controlling High-Order Hybrid Nanoparticle Morphology. *J. Am. Chem. Soc.* **2015,** *137* (49), 15493-15500.

(6) Chen, P. C.; Du, J. S. S.; Meckes, B.; Huang, L. L.; Xie, Z.; Hedrick, J. L.; Dravid, V. P.; Mirkin, C. A., Structural Evolution of Three-Component Nanoparticles in Polymer Nanoreactors. *J. Am. Chem. Soc.* **2017,** *139* (29), 9876-9884.

(7) Peng, S.; Lei, C. H.; Ren, Y.; Cook, R. E.; Sun, Y. G., Plasmonic/Magnetic Bifunctional Nanoparticles. *Angew. Chem. Int. Ed.* **2011,** *50* (14), 3158-3163.

(8) Wanjala, B. N.; Luo, J.; Loukrakpam, R.; Fang, B.; Mott, D.; Njoki, P. N.; Engelhard, M.; Naslund, H. R.; Wu, J. K.; Wang, L. C.; Malis, O.; Zhong, C. J., Nanoscale Alloying, Phase-Segregation, and Core-Shell Evolution of Gold-Platinum Nanoparticles and Their Electrocatalytic Effect on Oxygen Reduction Reaction. *Chem. Mater.* **2010,** *22* (14), 4282-4294.

(9) Suntivich, J.; Xu, Z. C.; Carlton, C. E.; Kim, J.; Han, B. H.; Lee, S. W.; Bonnet, N.; Marzari, N.; Allard, L. F.; Gasteiger, H. A.; Hamad-Schifferli, K.; Shao-Horn, Y., Surface Composition Tuning of Au-Pt Bimetallic Nanoparticles for Enhanced Carbon Monoxide and Methanol Electro-oxidation. *J. Am. Chem. Soc.* **2013,** *135* (21), 7985-7991.

(10) Zafeiratos, S.; Piccinin, S.; Teschner, D., Alloys in catalysis: phase separation and surface segregation phenomena in response to the reactive environment. *Catal. Sci. Technol.* **2012,** *2* (9), 1787-1801.

(11) Konuspayeva, Z.; Berhault, G.; Afanasiev, P.; Nguyen, T. S.; Giorgio, S.; Piccolo, L., Monitoring in situ the colloidal synthesis of AuRh/TiO2 selective-hydrogenation nanocatalysts. *J. Mater. Chem. A* **2017,** *5* (33), 17360-17367.

(12) Piccolo, L.; Li, Z. Y.; Demiroglu, I.; Moyon, F.; Konuspayeva, Z.; Berhault, G.; Afanasiev, P.; Lefebvre, W.; Yuan, J.; Johnston, R. L., Understanding and controlling the structure and segregation behaviour of AuRh nanocatalysts. *Sci. Rep.* **2016,** *6*, 35226.

(13) Zhang, X. B.; Han, S. B.; Zhu, B. E.; Zhang, G. H.; Li, X. Y.; Gao, Y.; Wu, Z. X.; Yang, B.; Liu, Y. F.; Baaziz, W.; Ersen, O.; Gu, M.; Miller, J. T.; Liu, W., Reversible loss of core-shell structure for Ni-Au bimetallic nanoparticles during CO_2 hydrogenation. *Nat. Catal.* **2020,** *3* (4), 411-417.

(14) Divins, N. J.; Angurell, I.; Escudero, C.; Perez-Dieste, V.; Llorca, J., Influence of the support on surface rearrangements of bimetallic nanoparticles in real catalysts. *Science* **2014,** *346* (6209), 620-623.

(15) Kim, D.; Nam, H.; Cho, Y. H.; Yeo, B. C.; Cho, S. H.; Ahn, J. P.; Lee, K. Y.; Lee, S. Y.; Han, S. S., Unlocking the Potential of Nanoparticles Composed of Immiscible Elements for Direct H_2O_2 Synthesis. *ACS Catal.* **2019,** *9* (9), 8702-8711.

(16) Chen, P. C.; Liu, G. L.; Zhou, Y.; Brown, K. A.; Chernyak, N.; Hedrick, J. L.; He, S.; Xie, Z.; Lin, Q. Y.; Dravid, V. P.; O'Neill-Slawecki, S. A.; Mirkin, C. A., Tip-Directed Synthesis of Multimetallic Nanoparticles. *J. Am. Chem. Soc.* **2015,** *137* (28), 9167-9173.

(17) Chen, P. C.; Liu, X. L.; Hedrick, J. L.; Xie, Z.; Wang, S. Z.; Lin, Q. Y.; Hersam, M. C.; Dravid, V. P.; Mirkin, C. A., Polyelemental nanoparticle libraries. *Science* **2016,** *352* (6293), 1565-1569.

(18) Chen, P. C.; Liu, M. H.; Du, J. S. S.; Meckes, B.; Wang, S. Z.; Lin, H. X.; Dravid, V. P.; Wolverton, C.; Mirkin, C. A., Interface and heterostructure design in polyelemental nanoparticles. *Science* **2019,** *363* (6430), 959-964.

(19) Langlois, C.; Li, Z. L.; Yuan, J.; Alloyeau, D.; Nelayah, J.; Bochicchio, D.; Ferrando, R.; Ricolleau, C., Transition from core-shell to Janus chemical configuration for bimetallic nanoparticles. *Nanoscale* **2012,** *4* (11), 3381-3388.

(20) Shubin, Y.; Plyusnin, P.; Sharafutdinov, M.; Makotchenko, E.; Korenev, S., Successful synthesis and thermal stability of immiscible metal Au-Rh, Au-Ir and Au-Ir-Rh nanoalloys. *Nanotechnology* **2017,** *28* (20), 205302.

(21) Fevre, M.; Le Bouar, Y.; Finel, A., Thermodynamics of phase-separating nanoalloys: Single particles and particle assemblies. *Phys. Rev. B* **2018,** *97* (19), 195404.

(22) Pohl, J.; Stahl, C.; Albe, K., Size-dependent phase diagrams of metallic alloys: A Monte Carlo simulation study on order-disorder transitions in Pt-Rh nanoparticles. *Beilstein J. Nanotechnol.* **2012,** *3*, 1-11.

(23) Feng, J. C.; Chen, D.; Pikhitsa, P. V.; Jung, Y. H.; Yang, J.; Choi, M., Unconventional Alloys Confined in Nanoparticles: Building Blocks for New Matter. *Matter* **2020,** *3* (5), 1646-1663.

(24) Srivastava, C.; Chithra, S.; Malviya, K. D.; Sinha, S. K.; Chattopadhyay, K., Size dependent microstructure for Ag-Ni nanoparticles. *Acta Mater.* **2011,** *59* (16), 6501-6509.

(25) Radnoczi, G.; Bokanyi, E.; Erdelyi, Z.; Misjak, F., Size dependent spinodal decomposition in Cu-Ag nanoparticles. *Acta Mater.* **2017,** *123*, 82-89.

(26) Xiao, S.; Hu, W.; Luo, W.; Wu, Y.; Li, X.; Deng, H., Size effect on alloying ability and phase stability of immiscible bimetallic nanoparticles. *European Physical Journal B* **2006,** *54* (4), 479-484.

(27) Qi, W. H.; Wang, M. P., Size effect on the cohesive energy of nanoparticle. *J. Mater. Sci. Lett.* **2002,** *21* (22), 1743-1745.

(28) Rajeeva, B. B.; Kunal, P.; Kollipara, P. S.; Acharya, P. V.; Joe, M.; Ide, M. S.; Jarvis, K.; Liu, Y. Y.; Bahadur, V.; Humphrey, S. M.; Zheng, Y. B., Accumulation-Driven Unified Spatiotemporal Synthesis and Structuring of Immiscible Metallic Nanoalloys. *Matter* **2019,** *1* (6), 1606-1617.

(29) Roling, L. T.; Mavrikakis, M., Toward rational nanoparticle synthesis: predicting surface intermixing in bimetallic alloy nanocatalysts. *Nanoscale* **2017,** *9* (39), 15005-15017.

(30) Liao, H. B.; Fisher, A.; Xu, Z. C. J., Surface Segregation in Bimetallic Nanoparticles: A Critical Issue in Electrocatalyst Engineering. *Small* **2015,** *11* (27), 3221-3246.

(31) Sneed, B. T.; Young, A. P.; Tsung, C. K., Building up strain in colloidal metal nanoparticle catalysts. *Nanoscale* **2015,** *7* (29), 12248-12265.

(32) Panizon, E.; Ferrando, R., Strain-induced restructuring of the surface in core@shell nanoalloys. *Nanoscale* **2016,** *8* (35), 15911-15919.

(33) Najafishirtari, S.; Guardia, P.; Scarpellini, A.; Prato, M.; Marras, S.; Manna, L.; Colombo, M., The effect of Au domain size on the CO oxidation catalytic activity of colloidal Au-FeOx dumbbell-like heterodimers. *J. Catal.* **2016,** *338*, 115-123.

(34) Xie, C. L.; Chen, C.; Yu, Y.; Su, J.; Li, Y. F.; Somorjai, G. A.; Yang, P. D., Tandem Catalysis for CO2 Hydrogenation to C-2-C-4 Hydrocarbons. *Nano Lett.* **2017,** *17* (6), 3798-3802.

(35) Ha, M. J.; Kim, J. H.; You, M.; Li, Q.; Fan, C. H.; Nam, J. M., Multicomponent Plasmonic Nanoparticles: From Heterostructured Nanoparticles to Colloidal Composite Nanostructures. *Chem. Rev.* **2019,** *119* (24), 12208-12278.

(36) Lin, M.; Kim, G. H.; Kim, J. H.; Oh, J. W.; Nam, J. M., Transformative Heterointerface Evolution and Plasmonic Tuning of Anisotropic Trimetallic Nanoparticles. *J. Am. Chem. Soc.* **2017,** *139* (30), 10180-10183.

(37) Figuerola, A.; Fiore, A.; Di Corato, R.; Falqui, A.; Giannini, C.; Micotti, E.; Lascialfari, A.; Corti, M.; Cingolani, R.; Pellegrino, T.; Cozzoli, P. D.; Manna, L., One-pot synthesis and characterization of size-controlled bimagnetic FePt-iron oxide heterodimer nanocrystals. *J. Am. Chem. Soc.* **2008,** *130* (4), 1477-1487.

(38) Yu, H.; Chen, M.; Rice, P. M.; Wang, S. X.; White, R. L.; Sun, S. H., Dumbbell-like bifunctional Au-Fe3O4 nanoparticles. *Nano Lett.* **2005,** *5* (2), 379-382.

(39) Rodriguez-Fernandez, D.; Langer, J.; Henriksen-Lacey, M.; Liz-Marzan, L. M., Hybrid Au-SiO2 Core-Satellite Colloids as Switchable SERS Tags. *Chem. Mater.* **2015,** *27* (7), 2540-2545.

(40) Okamoto, H.; Schlesinger, M. E.; Mueller, E. M. Eds. *Alloy Phase Diagrams*; ASM Handbook Vol.3; ASM International: Materials Park, OH, U.S.A., 2016.

(41) Ethirajan, A.; Punniyakoti, S.; D'Olieslaeger, M.; Wagner, P.; Boyen, H. G., Ultrafast Self-Assembly Using Ultrasound: A Facile Route to the Rapid Fabrication of Well-Ordered Dense Arrays of Inorganic Nanostructures. *Angew. Chem. Int. Ed.* **2013,** *52* (37), 9709-9713.

(42) Dunn, K. W.; Kamocka, M. M.; McDonald, J. H., A practical guide to evaluating colocalization in biological microscopy. *Am. J. Physiol. Cell Physiol.* **2011,** *300* (4), C723-C742.

(43) Yang, Y. S.; Chen, C. C.; Scott, M. C.; Ophus, C.; Xu, R.; Pryor, A.; Wu, L.; Sun, F.; Theis, W.; Zhou, J. H.; Eisenbach, M.; Kent, P. R. C.; Sabirianov, R. F.; Zeng, H.; Ercius, P.; Miao, J.

W., Deciphering chemical order/disorder and material properties at the single-atom level. *Nature* **2017,** *542* (7639), 75-79.

(44) Pryor, A.; Yang, Y.; Rana, A.; Gallagher-Jones, M.; Zhou, J. H.; Lo, Y. H.; Melinte, G.; Chiu, W.; Rodriguez, J. A.; Miao, J. W., GENFIRE: A generalized Fourier iterative reconstruction algorithm for high-resolution 3D imaging. *Sci. Rep.* **2017,** *7*, 10409.

(45) Buendia, F.; Vargas, J. A.; Johnston, R. L.; Beltran, M. R., Study of the stability of small AuRh clusters found by a Genetic Algorithm methodology. *Comput. Theor. Chem.* **2017,** *1119*, 51-58.

(46) Mezey, L. Z.; Giber, J., The Surface Free Energies of Solid Chemical Elements: Calculation from Internal Free Enthalpies of Atomization. *Jpn. J. Appl. Phys., Part 1* **1982,** *21* (11), 1569-1571.

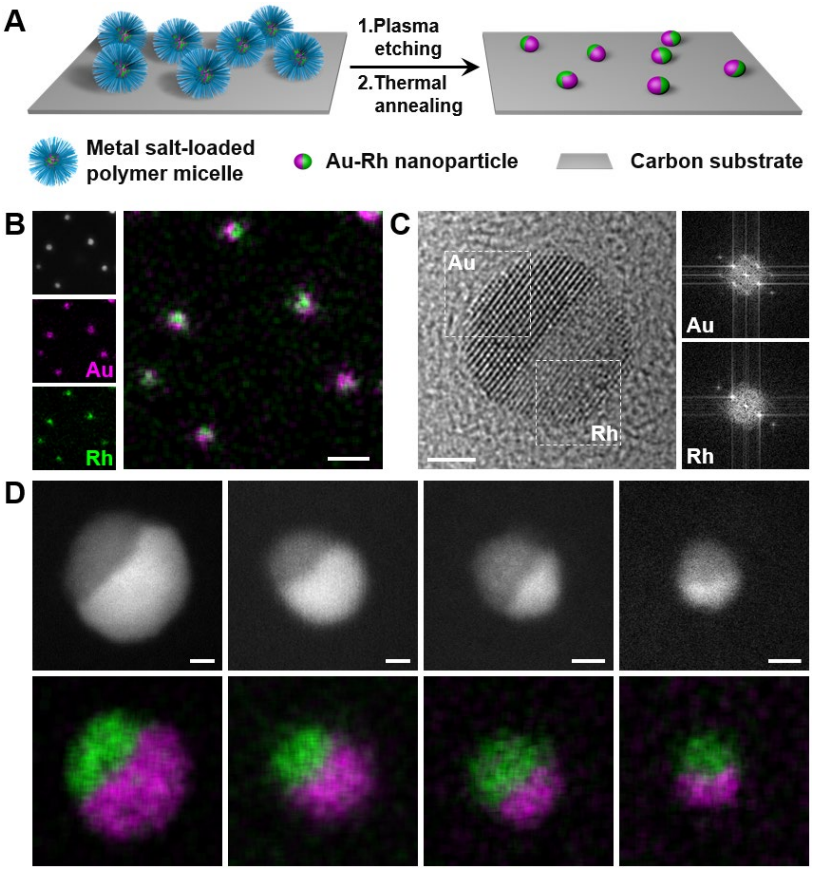

Figure 1. Micelle-mediated synthesis of AuRh nanoparticles. (A) Scheme of the micelle-mediated nanoparticle synthesis. (B) HAADF-STEM images and EDS elemental maps of AuRh nanoparticles synthesized in micelle reactors. Scale bar: 10 nm. (C) HRTEM image of a AuRh nanoparticle and FFT of the regions indicated by dashed squares in the HRTEM image. Scale bar: 2 nm. (D) HAADF-STEM images and EDS elemental maps of individual AuRh nanoparticles with size between 4–12 nm. Scale bars: 2 nm.

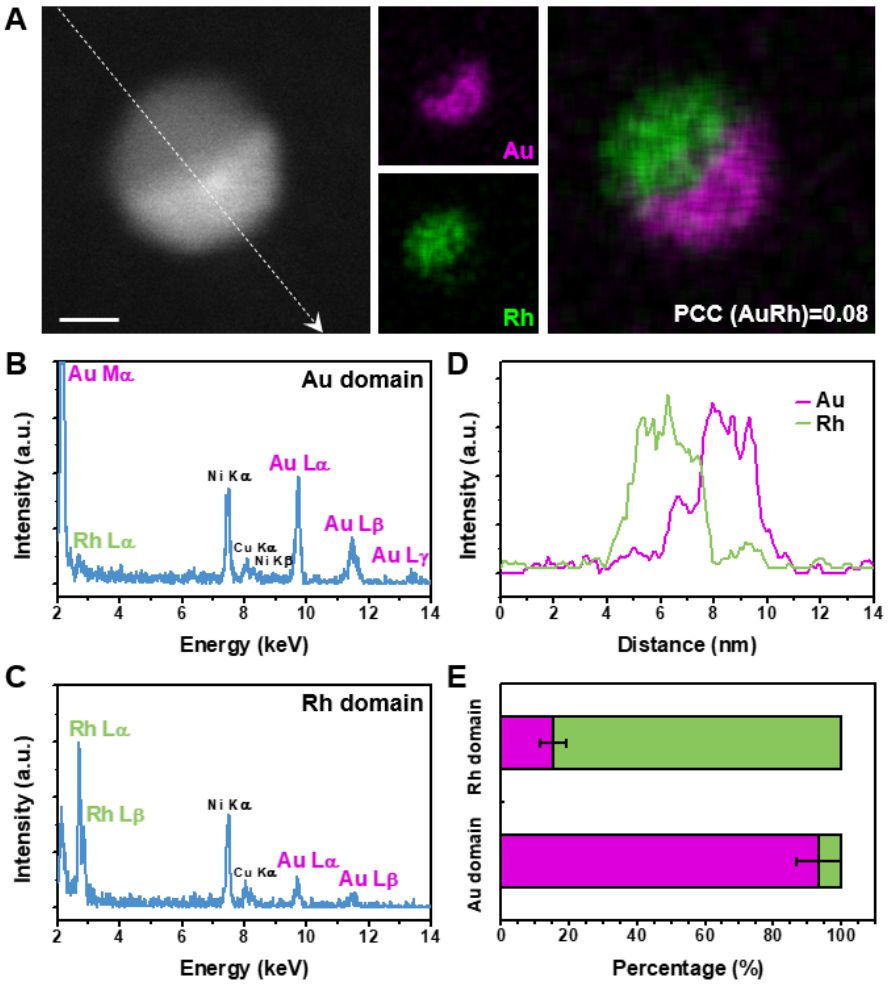

Figure 2. EDS analysis of the Au-Rh phase separation in nanoparticles. (A) HAADF-STEM image and EDS elemental maps of a representative AuRh nanoparticle. The Pearson's correlation coefficient (PCC) of the Au and Rh maps is 0.08, suggesting phase separation between the majority of Au and Rh atoms. Scale bar: 2 nm. (B,C) EDS spectra of the Au and Rh domains of the nanoparticle shown in (A). (D) EDS line-scan profile across the Au and Rh domains of the nanoparticles in (A). The white arrow in (A) shows the trace of the line scan. (E) Atomic composition of the Au and Rh domains in AuRh nanoparticles that is assessed from 25 particles with size between 4–12 nm.

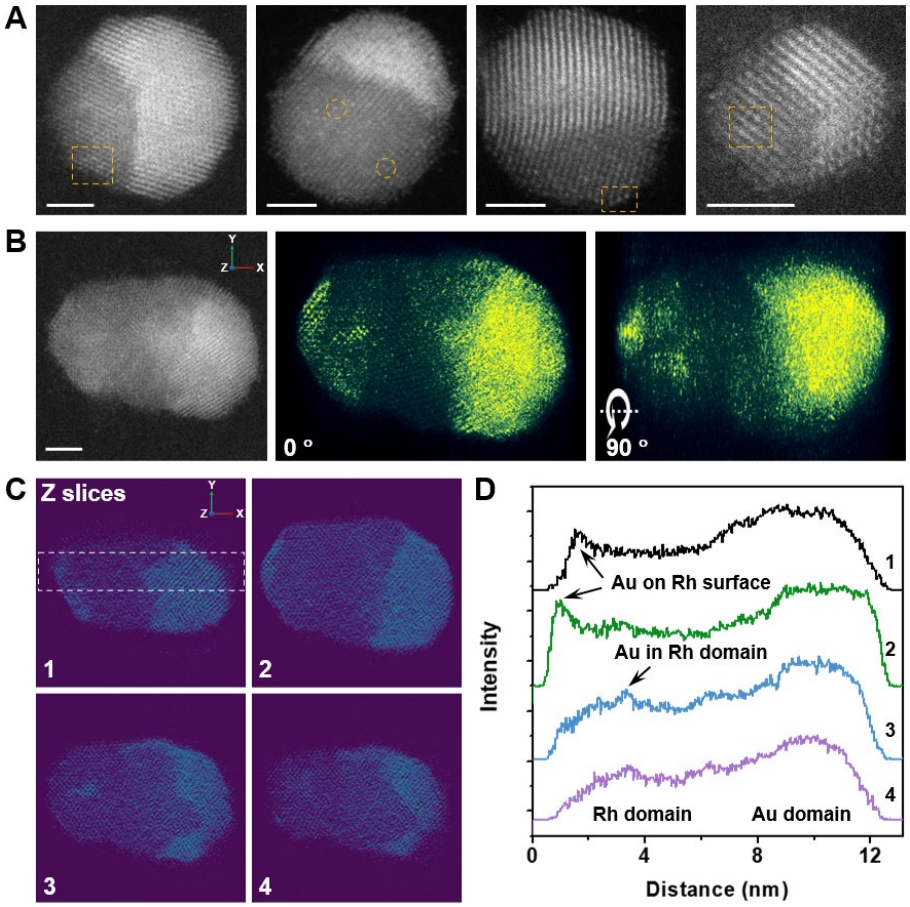

Figure 3. Distribution of Au and Rh atoms in Au-Rh nanoparticles. (A) High-resolution HAADF-STEM images of AuRh nanoparticles. Yellow dashed rectangles and circles highlight the Au clusters and single atoms in the Rh domains, respectively. Scale bars: 2 nm. (B) Aberration-corrected STEM image and 3D-reconstructed result of a AuRh nanoparticle. The bright atoms in the reconstructed image represent Au. The intensity histogram of the associated color map is modified to suppress the low-intensity pixels, so that Au-rich domain is highlighted. Scale bar: 2 nm. (C) Z-sections of the nanoparticle shown in (B). The Z direction is perpendicular to the image plane of the nanoparticle. (D) Intensity profiles of the regions indicated by the white dashed rectangle in the Z-section images in (C).

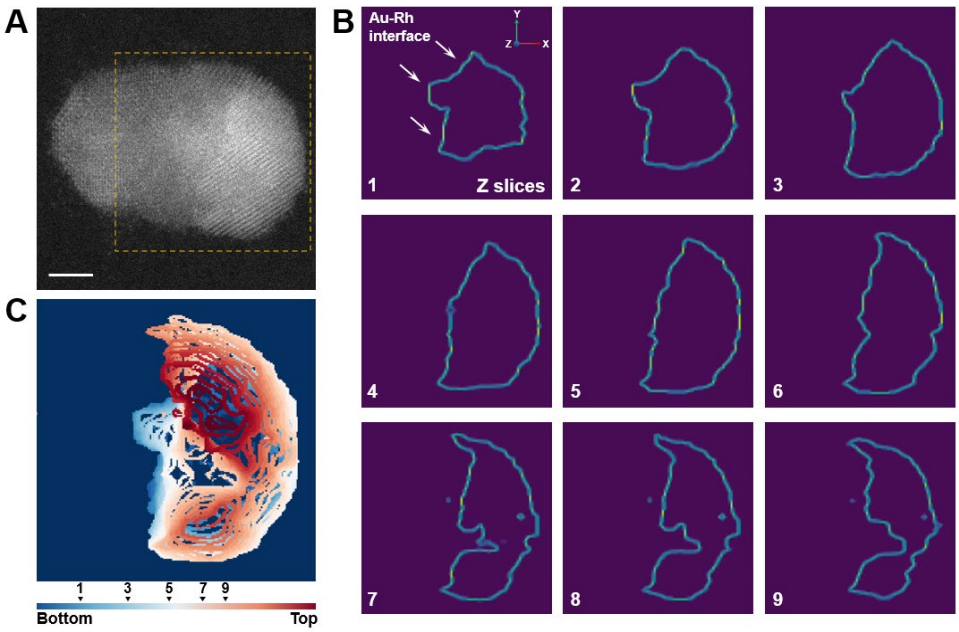

Figure 4. Interface analysis of Au-Rh nanoparticles. (A) HAADF-STEM image of the AuRh nanoparticle used for 3D reconstruction. Scale bar: 2 nm. Yellow dashed square highlights the uneven interface. (B) Contour lines of the Au domain at different Z height. The Z direction is perpendicular to the image plane of the nanoparticle in (A). (C) Overlay of the contour lines of the Au domain at different Z positions. The Z positions of the images in (B) are indicated on the color bar.

Table of Contents Graphic

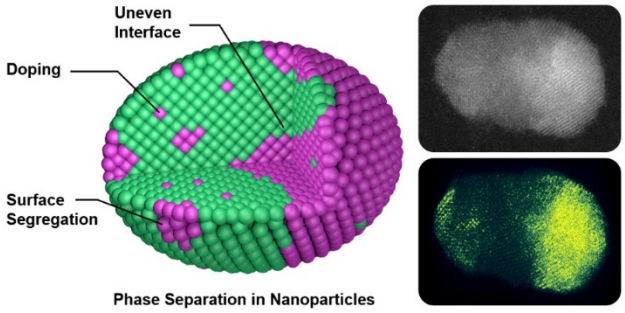

Phase Separation in Nanoparticles